PHYSICAL REVIEW B VOLUME 36, NUMBER 13 1 NOVEMBER 1987

Resonant scattering and Anderson localization of acoustic waves

C. A. Condat*
Institute for Physical Science and Technology, University of Maryland, College Park, Maryland 20742

T. R. Kirkpatrick
Department of Physics and Astronomy, University of Maryland, College Park, Maryland 20742
and Institute for Physical Science and Technology, University of Maryland, College Park, Maryland 20742
(Received 2 April 1987)

The properties of an acoustical medium containing a random array of identical discrete scatterers are investigated in detail. The cases of hard scatterers, soft scatterers, and permeable scatterers are considered for two- and three-dimensional configurations. Curves describing the diffusion coefficient, the localization length, and the phase boundaries are presented and the results are related to the single-scattering properties. The consequences of a modification in the self-consistent theory cutoff are examined. The onset of localization in three dimensions is shown to satisfy approximately the Ioffe-Regel condition.

I. INTRODUCTION

It has been shown[1] that it should not be too difficult to localize acoustic waves in a three-dimensional composite formed by two media whose acoustic indices of refraction are different enough. This prediction contrasts with that for hard-sphere acoustical scatterers, which are probably incapable of localizing acoustic waves.[2] It is, therefore, interesting to explore in detail how the properties of individual scatterers can affect the intensity of localization phenomena. We have started this investigation with a description of how the frequency dependence of some parameters that play an important role in the analyses of localization (renormalized speed of sound, scattering and transport mean free paths) varies when the characteristics of the scatterers are modified.[3] In that work, hereafter to be referred as I, we showed explicitly the connection between the structure of the frequency dependence of these parameters and that of the total scattering cross section.

Considerable progress has been made in the study of acoustic localization in one-dimensional disordered media (a case in which all excitations, except, perhaps, for a set of measure zero,[4] are predicted to be localized). Dépollier, Kergomard, and Laloe[5] have found evidence for localization studying acoustic waves in a long pipe. The disorder was introduced by a series of randomly ordered, resonant, closed branches that emerged periodically to the main pipe. These authors have also reviewed the previous one-dimensional work. He and Maynard[6] studied the transverse excitations of a steel wire along which a set of small, identical masses were attached in random positions. They also found strong evidence for localization.

Some time ago, we proposed an experiment to localize third-sound waves on a helium film adsorbed on a disordered substrate.[4,7] The "index of refraction" scatterers of Ref. 4 are the one-dimensional analogs of some of the scatterers to be discussed in this paper. The work in higher-dimensional systems has been mostly theoretical. John, Sompolinsky, and Stephen[8] used a field-theoretical method to study the transition from extended to localized states in a disordered elastic medium. Kirkpatrick[9] adapted the self-consistent theory[10] (SCT) to analyze the localization of sound by hard-disk and hard-sphere scatterers. The properties of third sound in a two-dimensional (2D) disordered configuration as well as the influence of flow on one- and two-dimensional localized acoustic excitations have also been investigated theoretically.[11–13] The intensity fluctuations (speckle pattern), described by the intensity-intensity correlation function, have been studied by Shapiro.[14] Flesia, Johnston, and Kunz[15] performed a numerical analysis of the propagation of waves through a network of wave guides with a randomly varying index of refraction.

The study of the localization of electromagnetic (EM) waves, on the other hand, has received a great impulse due to several successful experiments on the enhanced coherent backscattering of light.[16–22] This phenomenon is considered a precursor of Anderson localization. Closely related is Genack's measurement of the parameters of optical propagation in a wedged random medium.[23] Although not performed with the idea of localization in mind, some older experiments on the backscattering of light and sound by random media, described in the review paper by Kravtsov and Saichev,[24] are also relevant. The theoretical literature related to EM coherent backscattering and localization is also vast.[24–31] Although the EM problem has been often treated in the framework of a scalar wave equation, polarization effects must be accounted for if a complete understanding of the resonant backscattering experiments is desired.[29,30]

The problem of the localization of classical waves in the presence of finite scatterers was first analyzed in Ref. 9. It was there pointed out that since the boundary conditions for sound waves incident on hard spheres are of the Neumann type, there would be important qualitative

 ©1987 The American Physical Society

differences with respect to the case of electrons in a Lorentz gas, for the electron wave function satisfies Dirichlet boundary conditions at the surfaces of the scatterers. At high frequencies the Dirichlet and Neumann scattering cross sections are equivalent; a delocalization tendency occurs in both cases due to the compactness of the excitations, which in $d=3$ can easily diffuse through the inhomogeneous medium. At low frequencies the Dirichlet scattering cross section goes to a constant, leading to low-energy electron localization. On the other hand, the Neumann cross section vanishes as E^{d+1} at small frequencies E. This makes the scattering very inefficient and the sound waves tend to be delocalized.

The analysis of the Neumann problem in Ref. 9 led to the conclusion that in two dimensions all states are localized, although the localization length ξ diverges rapidly at high and low frequencies. The possibility was suggested that for $d=3$ there could be a region of localized states at intermediate frequencies. Correspondingly, the existence of two mobility edges was predicted. In Ref. 2 we used the "pseudosphere" approximation (PA) to obtain quantitative predictions for the Neumann problem: While for $d=2$ values of ξ small enough to be observable are possible—at least at high scatterer densities—for $d=3$ the calculation suggests that all states are extended.

In their study of the localization characteristics of a two-component composite, Sheng and Zhang[1] showed that the situation is very different if the wave is allowed to penetrate the scatterers. If the relative index of refraction of the minority component is high enough, resonant behavior is possible and they predicted the existence of a multiplicity of localization regions and mobility edges. Arya, Su, and Birman[31] studied the effect of the Mie resonances of metallic spheres on the localization of EM waves. They keep the vector character of the waves and consider explicitly the resonant behavior of the $l=1$ partial wave.

It is therefore important to make a comparative analysis of how the different characteristics of various types of scatterers influence the localization phenomena. Here we apply the SCT to describe the diffusion or localization of acoustic excitations in the type of two- and three-dimensional disordered media described in I.

In Sec. II we put forward the models to be considered and describe the similarities and differences with respect to the model used in Ref. 1. The theoretical formulation of the solution to the localization problem is then briefly discussed. The explicit results for the three-dimensional case are presented in Sec. III, where the phase diagrams, localization lengths, and diffusion coefficients resulting from the various models are evaluated. The diffusion coefficient is also plotted in terms of the Ioffe-Regel parameter [(wave number)$\times$(transport mean free path)], which yields information on the approach to the mobility edges. The results for the two-dimensional models are obtained and analyzed in Sec. IV. Throughout, the properties of the excitations in the disordered media are related to the characteristics of the individual scatterers. Some further analyses are made in Sec. V.

We have neglected dissipative effects completely. This is a reasonable approximation if the inelastic scattering length l_i is much larger than the scattering mean free path. Of course, localization will be observed only if the localization length is also shorter than l_i.[32] A simple way to estimate l_i was suggested in I. Various aspects of the problem of localization in media such that dissipation is nonnegligible were studied in Refs. 26 and 27.

II. MODELS AND FORMALISM

The models we will study are the same as those in I. We consider a collection of uncorrelated, identical, randomly distributed spherical (disklike if $d=2$) scatterers immersed in a uniform lossless medium. The radius of the scatterers is a and their number density is n. The dimensionless number densities (i.e., the volume fractions) are $n^*=\pi a^2 n$ $(d=2)$ and $n^*=(\frac{4}{3})\pi a^3 n$ $(d=3)$. The background medium is characterized by a mass density ρ and a compressibility κ. The pressure waves can be described using a velocity potential $\phi(\mathbf{x},t)$, which in the absence of scatterers satisfies the wave equation

$$\left[\frac{\partial^2}{\partial t^2}-c^2\nabla^2\right]\phi(\mathbf{x},t)=0\ , \tag{2.1}$$

where $c=(1/\kappa\rho)^{1/2}$ is the speed of sound.

We will analyze the localization phenomena for pressure waves in the presence of three types of scatterers, whose properties can be expressed through appropriate boundary conditions.

(a) Hard (Neumann) scatterers: These are considered in Refs. 2 and 9. The fluid velocity normal to the scatterers vanishes and this leads to the vanishing of the radial derivative of ϕ at $r=a$.

(b) Soft (Dirichlet) scatterers: As mentioned before, an electronic wave function satisfies a Dirichlet condition at the surface of an impenetrable sphere. This is also the case for pressure waves scattered by an ideally rigid, empty bubble, at whose surface the pressure, and thus ϕ, must vanish.

(c) Permeable scatterers: The wave is allowed to penetrate the scatterers, which are characterized by a mass density ρ_s and a compressibility κ_s. (The subscript s will indicate a magnitude associated with the scatterers.) As in I, we find it convenient to describe the scatterers in terms of the density ratio, $\Delta=\rho/\rho_s$, and the index of refraction, $M=c/c_s=(\rho_s\kappa_s/\rho\kappa)^{1/2}$. The case $\Delta=1$, $M>1$, which, as we will see, yields the most interesting behavior, was considered in Ref. 1. The requirements of continuity in the pressure and normal component of the fluid velocity generate the boundary conditions at $r=a$,

$$\phi_s=\phi\Delta\ ,$$
$$\frac{\partial\phi_s}{\partial r}=\frac{\partial\phi}{\partial r}\ .$$

We will not consider here solid scatterers, for which a description in terms of ρ_s and κ_s is not complete. In this case two different wave numbers, corresponding to compression and shear modes, enter the description and the formulas became considerably more involved. Our

description is accurate for fluid scatterers and for solids such as silicone rubber, for which there is negligible shear conversion at the scatterer surface.[33]

Sheng and Zhang[1] considered scatterers having different compressibility from that of the surrounding medium. They combined the SCT with an effective-medium approximation and treated the two components of a composite on an equal footing. This treatment is appropriate when the volume fraction of the minority component is close to or beyond that of the percolation threshold; in this case there would be what can be schematically thought of as a large admixture of the wave traveling in component A and being scattered by B with that traveling in component B and being scattered by A. If the density of the minority component is below, and not too close to, that of the percolation threshold, we feel that it is better not to make the effective-medium approximation and to consider the excitation as propagating in the majority matrix and being scattered by spherical inclusions. This is the case we consider here. Although our results are perfectly compatible with those of the effective medium, there are some differences; in particular, we predict the onset of localization at lower values of the density of the minority component.

The analysis of wave propagation and localization in a random medium makes use of two equations which can be discussed in terms of diagrams:[9,34] the Dyson equation, satisfied by the configurational average $\langle G \rangle$ of the Green's function, and the Bethe-Salpeter equation, satisfied by the average $\langle GG \rangle$ of a product of Green's functions. In particular, the spectral components of the velocity potential at $(\mathbf{x},t)$ generated by a point source at $(\mathbf{x},0)$ are given by the averaged retarded Green's function

$$\langle G_E^+(\mathbf{x},\mathbf{x}') \rangle = (2\pi)^{-d} \int d\mathbf{k} \frac{e^{i\mathbf{k}\cdot(\mathbf{x}-\mathbf{x}')}}{E^2 - c^2 k^2 - \Sigma_{\mathbf{k}}(E)} . \tag{2.2}$$

At low scatterer densities, the self-energy can be written in terms of the diagonal elements of the T matrix[9]

$$\Sigma_{\mathbf{k}}(E) \cong (2\pi)^d n \langle \mathbf{k} \mid \hat{T}(E) \mid \mathbf{k} \rangle \equiv \gamma_{\mathbf{k}}(E) \mp i\sigma_{\mathbf{k}}(E) . \tag{2.3}$$

The real and imaginary parts of the self-energy lead, respectively, to a renormalization of the speed of sound and to a randomness-related attenuation of the excitations. These effects and their connections to the individual properties of the scattering centers were discussed at length in I. Here we note that the renormalized speed of sound $\tilde{c}(E)$ is defined as

$$\frac{1}{[\tilde{c}(E)]^2} = \frac{1}{c^2} \left[1 - \frac{1}{E^2} \gamma_{E/c} \right] , \tag{2.4}$$

while the attenuation length obtained from $\sigma_{\mathbf{k}}(E)$ is equivalent to the scattering mean free path $l_{sc} = (nS)^{-1}$. We call S to the total scattering cross section for a single scatterer.

Due to energy conservation, it can be shown that the energy density propagator, $\langle P_E \rangle$, which is the Fourier-Laplace transform of the averaged double Green's function, is proportional to a diffusive hydrodynamical pole,[9]

$$\langle P_E(\mathbf{q},\omega) \rangle \sim \frac{1}{-i\omega + D(E,\omega) q^2} . \tag{2.5}$$

Here $q,\omega \to 0$. We are interested in the properties of the diffusion coefficient $D(E,\omega)$ when the external frequency $\omega \to 0$. In this limit, $D(E,\omega)$ describes the diffusion of energy at very long times and its behavior will thus provide the information we require about localization.

The Bethe-Salpeter equation can be solved making a perturbative diagrammatic expansion of the energy density propagator. If only the ladder diagrams—and thus incoherent processes—are kept, we get the "Boltzmann equation" value for the diffusion coefficient:

$$D(E,\omega \to 0) = D_B(E) .$$

This approximation is appropriate if n^* is very small or if the scattering is weak (i.e., if $\Delta \cong 1$ and $M \cong 1$). As we will see, it is also suitable for low frequenecies (except in the Dirichlet case) and very high frequencies. The function $D_B(E)$ is used to define a transport mean free path, $l_T = dD_B(E)/c$, whose properties were also analyzed extensively in I.

To describe the "weak localization" phenomena investigated in Refs. 16–24, it is necessary to include in the perturbative expansion the contribution due to the constructive interference of conjugate waves traveling in opposite directions along the same closed path. The relevance of these coherent processes to the backscattering of waves from a disordered medium was first discussed by Watson in his investigation of the multiple scattering in a plasma.[35] This problem was further studied by de Wolf[36] and Barabanenkov.[37] This last author expressed the coherent contributions in a diagrammatic language, in terms of the cyclical or maximally crossed diagrams (MCD). A few years later, this phenomenon was found to be an essential component in the description of electron localization.[38]

Although successful to explain "weak localization," the perturbative approach is insufficient to describe the "strong" or Anderson localization. However, since the MCD represent coherent phenomena, they can be used as a starting point in the formulation of a self-consistent theory.[9,10] That this SCT is adequate can be verified by comparing its results with those of the exact Berezinskii calculation[13,39] (if $d = 1$) and of computer simulations.[40] We note that the SCT—at least in its usual form—does not give an accurate description if the time-reversal symmetry of the problem is broken. This would be the case, for example, if a flow is created in the background medium.[12,13]

The SCT leads to the following algebraic equation for the diffusion coefficient when $\omega \to 0$:[9]

$$D(E,\omega) = D_B(E) + \left[\frac{d\sigma_{E/c}(E) D_B(E)}{2\pi\Omega_d \tilde{c}^2} \right] \left[\frac{\tilde{c}}{E} \right]^d \times \int_0^Q \frac{d\mathbf{q}'}{i\omega D^{-1}(E,\omega) - (q')^2} . \tag{2.6}$$

Here $\Omega_1 = 1$, $\Omega_2 = \pi$, and $\Omega_3 = 2\pi$. A wave-number cutoff, Q, has been introduced. It is reasonable to as-

sume that $Q \sim l_T^{-1}$ since this is the wave-number scale where the $(q')^2$ approximation for the diffusion pole breaks down. However, within the SCT theory the ultraviolet cutoff is not uniquely given and other cutoffs are possible. For example, one could argue that $Q \sim a^{-1}$ so that the order of the leading density correction to D_B agrees with perturbation theory results.[41] Even if one insists that $Q \sim l_T^{-1}$ the proportionality constant is not known. We shall investigate below how different possible cutoffs affect our results numerically. We will write $Q = r d l_T^{-1}$, and analyze how our results depend on the value of r. In the Appendix we present the results for the case $Q = r a^{-1}$.

In Secs. III and IV we consider, separately, the three- and two-dimensional cases.

III. LOCALIZATION IN $d = 3$

The Anderson localization of acoustical excitations can be analyzed in terms of $D(E,\omega \to 0)$. In the frequency domains where the excitations are localized, $D(E,\omega \to 0)$ vanishes linearly in ω. Otherwise the excitations will be delocalized. In the delocalized regime, the ratio $D(E,\omega \to 0)/D_B(E)$ yields a convenient measure of the contribution of coherent effects. When this ratio is close to unity, the diffusion is mostly incoherent and the Boltzmann description is adequate. For values of E such that $D(E,\omega \to 0)/D_B(E) \ll 1$, coherent effects are strong and a mobility edge cannot be far away.

The relevant formulas are obtained immediately by combining the results from I and Ref. 9. Let us first define the following auxiliary functions:

$$\delta_l(\eta_s) = M \Delta j_l'(\eta_s)[j_l(\eta_s)]^{-1} ,$$
$$\alpha_l = j_l'(\eta) - \delta_l(\eta_s) j_l(\eta) , \tag{3.1}$$

and

$$f_l = y_l'(\eta) - \delta_l(\eta_s) y_l(\eta) .$$

Here $\eta = Ea/c$, $\eta_s = M\eta$, j_l, and y_l are spherical Bessel functions and the primes denote derivatives with respect to the argument.

The total scattering cross section is given by

$$S(\eta) = \frac{4\pi a^2}{\eta^2} \sum_{l=0}^{\infty} \frac{(2l+1)\alpha_l^2}{\alpha_l^2 + f_l^2} \equiv \frac{4\pi a^2}{\eta^2} S_1(\eta) . \tag{3.2}$$

The renormalized speed of sound is given by

$$\frac{1}{\tilde{c}^2} = \frac{1}{c^2}\left[1 + \frac{3\eta^*}{\eta^3} \sum_{l=0}^{\infty} \frac{(2l+1)\alpha_l f_l}{\alpha_l^2 + f_l^2}\right] , \tag{3.3}$$

and the Boltzmann diffusion coefficient is

$$D_B(\eta) = \frac{ac\eta^2}{9n^*}\left[\sum_{l=0}^{\infty}\left[\frac{(2l+1)\alpha_l^2}{(\alpha_l^2+f_l^2)} - \frac{2(l+1)\alpha_l\alpha_{l+1}(\alpha_l\alpha_{l+1}+f_l f_{l+1})}{(\alpha_l^2+f_l^2)(\alpha_{l+1}^2+f_{l+1}^2)}\right]\right]^{-1} \equiv \frac{ac\eta^2}{9n^* S_2(\eta)} . \tag{3.4}$$

These formulas are valid for permeable scatterers. The Neumann and Dirichlet cases are obtained by letting $\alpha_l = j_l'$, $f_l = y_l'$, and $\alpha_l = j_l$, $f_l = y_l$, respectively.

The total cross sections for several scatterer types are depicted in Fig. 1. While the cross sections for Dirichlet and Neumann boundary conditions are monotonous and featureless, those for low speed ($M > 1$) scatterers show peaks whose size increases with M. These peaks are generally due to the vanishing of f_l in one of the terms in Eq. (3.2). If there are peaks in the neighborhood of or below $\eta = 1$, they will be relevant because a large cross section in that range favors localization effects. For the same reason wave localization should occur for Dirichlet and be impossible for Neumann scatterers. Curves for $\tilde{c}(\eta)$ and for $D_B(\eta)$, or more precisely, for the transport mean free path $l_T(\eta) = dD_B/c$, were presented and discussed in I. We will now see how the properties of these functions determine the nature of the diffusion and localization processes.

The points on the phase boundary $n^{**}(\eta)$ separating localized and extended states in the (η, n^*) plane satisfy the equation

$$81(n^{**})^2 r S_1(\tilde{\eta}) S_2(\tilde{\eta}) = \pi \tilde{\eta}^6 . \tag{3.5}$$

Here $\tilde{\eta} = Ea/\tilde{c}$. We assume that the speed of sound is renormalized everywhere.

Let us now analyze Eq. (3.5). First we note that, roughly, $n^{**} \sim r^{-1/2}$: an increase in the cutoff decreases the minimum scatterer volume fraction compatible with localization. In Fig. 2 we show the phase boundary for three values of r when the scatterers are characterized by $\Delta = 1$ and $M = 2$. Although the curves have the same general shape, they are not obtained from each other by simply multiplying by a constant. The reason for this is that $\tilde{c}$ contains very rapid variations (see I) and so does the "rescaling" from $\tilde{\eta}$ to η. Even if this effect complicates the picture, it does not obscure the main features. We also note that $r = 2\pi/3$ corresponds to the choice of Sheng and Zhang.[1]

Equation (3.5) implies $\eta^{**} \sim \tilde{\eta}^3 (D_B/S)^{1/2}$. The factor $\tilde{\eta}^3$ is responsible for the delocalization of the high-frequency excitations. The minima of D_B (see Fig. 9 in I) occur at frequencies close to those of the maxima in S; this confirms the intuitively obvious conclusion that localization is favored by large cross sections. The renormalization of c causes the structure of n^{**} not to always follow that of S. For the sake of comparison we include in Fig. 2 a curve (for $r = 2\pi/3$) obtained using the unrenormalized speed of sound.

At low frequencies, Eq. (3.5) formally (the physical value of n^* cannot go above that for random close packing) goes to the limit

$$n^{**}\sim\tilde{\eta}^{-3}\left[\frac{r}{\pi}\left[(M^2\Delta-1)^2+\frac{3(1-\Delta)^2}{(2+\Delta)^2}\right]\left[(M^2\Delta-1)^2+\frac{3(1-\Delta)}{(2+\Delta)^2}-\frac{2(M^2\Delta-1)(1-\Delta)}{2+\Delta}\right]\right]^{-1/2}.$$

For N scatterers, $n^{**}\sim(16\pi/77r)^{1/2}\tilde{\eta}^{-3}$; for Dirichlet scatterers, $n^{**}\sim(\pi/81r)^{1/2}\tilde{\eta}$. These results indicate the localization of low-frequency excitations in the Dirichlet problem and the delocalization that occurs in all the other cases.

The phase boundaries for $\Delta=1$ and three values of M are shown in Fig. 3. It is evident that an increase in the index of refraction is followed by a fast increase in the size of the localization region. In Figs. 2 and 3 we have considered scatterers having the same density but higher compressibilities than the background medium. Scatterers having lower compressibilities than the background are much less efficient and generally do not lead to localization. This property, as well as the increase in the size of the localization region with increasing M, were already discussed by Sheng and Zhang in Ref. 1. As we found in Ref. 2, Neumann scatterers are also inefficient and do not lead to localization. If we select scatterers that have the compressibility of the background but different density, the localization effects are weak. In Fig. 4 we show the phase boundary for the $\Delta=0.25, M=2$ case, which corresponds to $\rho_s=4\rho$. The localized states are present only at high scatterer densities, even for the most favorable ($r=2\pi$) choice for the cutoff. In the same figure we present the Dirichlet phase boundary, which encompasses the low-frequency localized region.

The "pseudosphere" approximation (PA) used in Ref. 2 is equivalent to taking $S_2=S_1$ and thus neglecting the difference between l_{sc} and l_T. Since Arya, Su, and Birman[31] define the cutoff in terms of l_{sc}, their results are analogous to those obtained from our PA. The dot-dashed curve in Fig. 3 represents the PA phase boundary for $M=1.9$. For $\eta\lesssim 1$ this result is in a very good agreement with the "exact" curve. For higher values of η the phase boundary still mimicks the gross features of the exact curve, but suggests the onset of localization at substantially lower values of n^*. These conclusions can be inferred directly from the graphs for l_T and l_{sc} in I. These graphs also show that if $\eta\lesssim 1$ the differences should be more marked for Dirichlet scatterers. That this is indeed the case can be seen from Fig. 4. Denoting by n_p^{**} the values of the phase boundary obtained using the PA, we can write $n_p^{**}=n^{**}(l_{sc}/l_T)^{1/2}$.

The localized states are characterized by a localization length $\xi(E)$ defined by

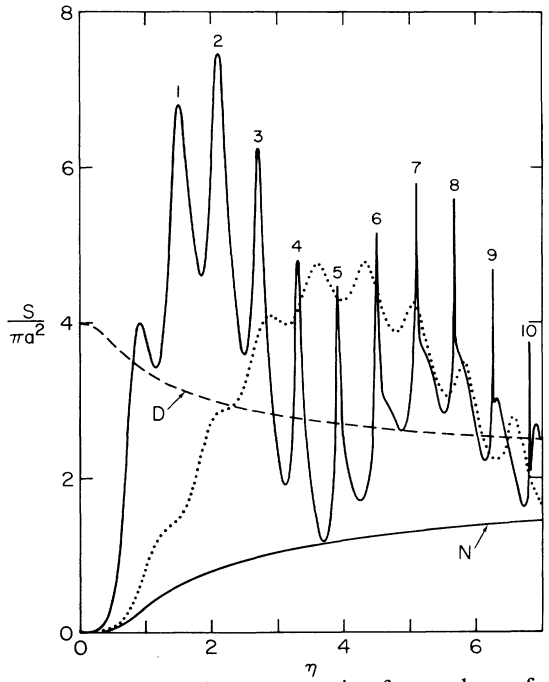

FIG. 1. Total scattering cross section for a sphere of radius a as a function of dimensionless frequency. The curves labeled D and N represent the Dirichlet and Neumann cases, respectively. The dotted line corresponds to ($\Delta=1$, $M=1.5$), while the structured solid line corresponds to ($\Delta=1$, $M=2$). The numbers above the peaks in the $M=2$ curve denote the value of l for the term originating the peak.

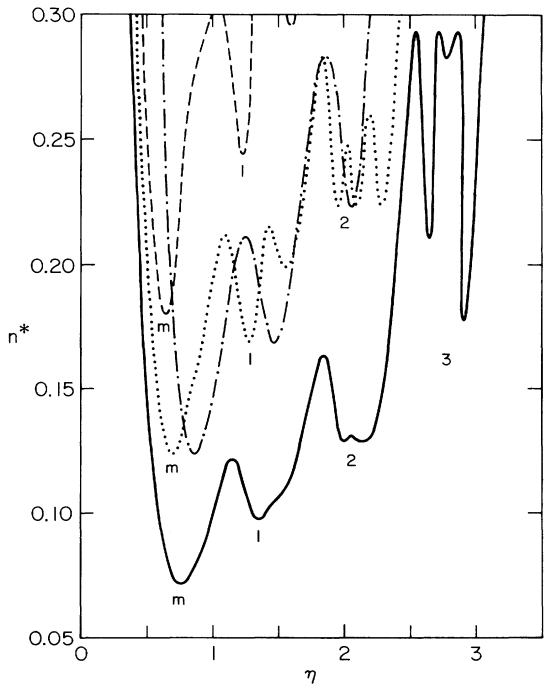

FIG. 2. Phase boundary for the case of scatterers of higher compressibility than the surrounding medium ($\Delta=1$, $M=2$). Three values were chosen for the cutoff: the solid line corresponds to $r=2\pi$, the dotted line to $r=2\pi/3$, and the dashed line to $r=1$. The numbers below the curves indicate the position of the features corresponding to the peaks in $S(\eta)$ (see Fig. 1). The minima corresponding to the first maxima in $S(\eta)$ are indicated by m. The results obtained for $r=2\pi/3$ using the unrenormalized speed of sound are represented by the dotted-dashed curve.

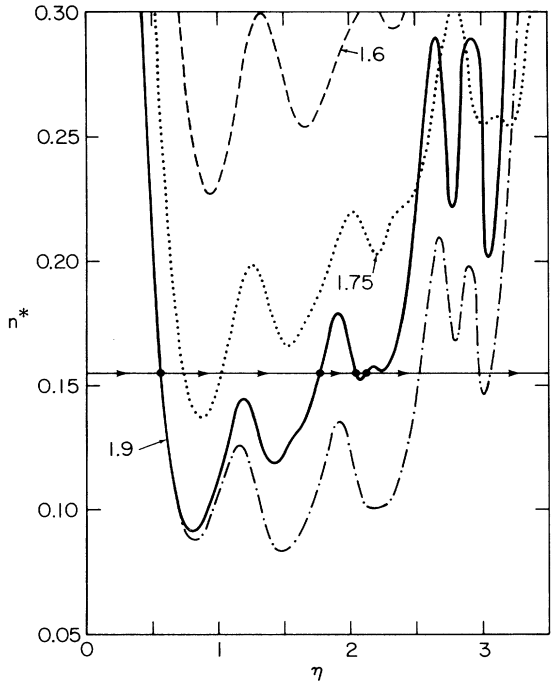

FIG. 3. Phase boundaries for scatterers characterized by $\Delta=1$ and three values of M, which label the corresponding curves. The "most favorable" ($r=2\pi$) cutoff has been chosen. Estimates for other values of r can be obtained by multiplying the curves by the factor $(2\pi/r)^{1/2}$. The horizontal line at $n^*=0.155$ represents the evolution of the parameter η as it generates the trajectory depicted in Fig. 8. The dotted-dashed curve is the pseudosphere approximation for $M=1.9$.

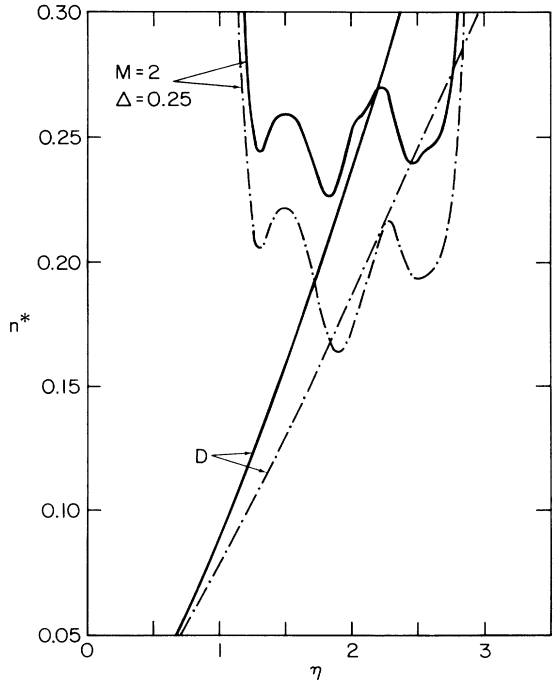

FIG. 4. Phase boundaries for the Dirichlet problem and for high density ($\rho_s=4\rho$) scatterers. As in the other cases, the localized states lie above the respective curves. We have taken $r=2\pi$. The dotted-dashed lines are the phase boundaries obtained using the PA.

$$D(E,\omega\to 0)=-i\omega\xi^2(E)+O(\omega^2)\ . \tag{3.6}$$

It is easy to verify that ξ satisfies

$$\left[1-\frac{\pi\tilde{\eta}^4}{9n^*QaS_1}\right]Q\xi=\arctan(Q\xi)\ . \tag{3.7}$$

Clearly $\xi\to\infty$ as we approach the phase boundary from the localized region.

The localization length is plotted in Fig. 5 for ($\Delta=1, M=1.75$) scatterers. The value of ξ decreases extremely fast as we move away from the phase boundary and into the localization region. The strong effect of varying the scatterer volume fraction n^* is also evident from the figure: A relatively small increase in n^* leads to a considerable shortening of the localization length. In the higher-density cases, the value of ξ/a decreases below unity. This seemingly unphysical result is due to the large size of the cutoff for those densities and frequencies. We believe that there should be a lower bound of the order of the interscatterer distance for ξ. It may be possible to introduce a crossover from a mean free path related cutoff to a cutoff defined in terms of the interscatterer distances. Since there is no compelling evidence for a definitive choice, we will not pursue this point further.

The diffusion of the extended excitations at long times is described in Fig. 6, where we have plotted $D(0)\equiv D(\eta,\omega\to 0)$ in units of the Boltzmann diffusion coefficient. The various curves have the same features, which become intensified as the density is increased. This result was to be expected, since the location of these features is determined by the properties of the individual scatterers. Two mobility edges are present for $n^*=0.14$ and four for $n^*=0.18$. The explicit form for the diffusion coefficient is

$$\frac{D(0)}{D_B}=1-\frac{81r(n^*)^2S_1S_2}{\pi\tilde{\eta}^6}\ . \tag{3.8}$$

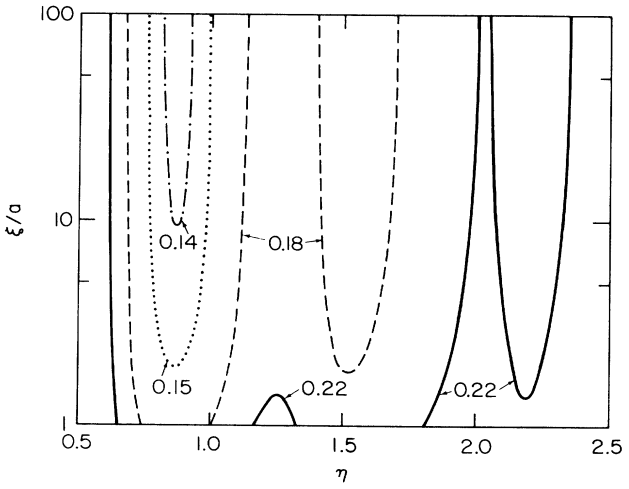

FIG. 5. Localization lengths for the volume fractions specified next to the corresponding curves. We have taken $\Delta=1$, $M=1.75$, and $r=2\pi$.

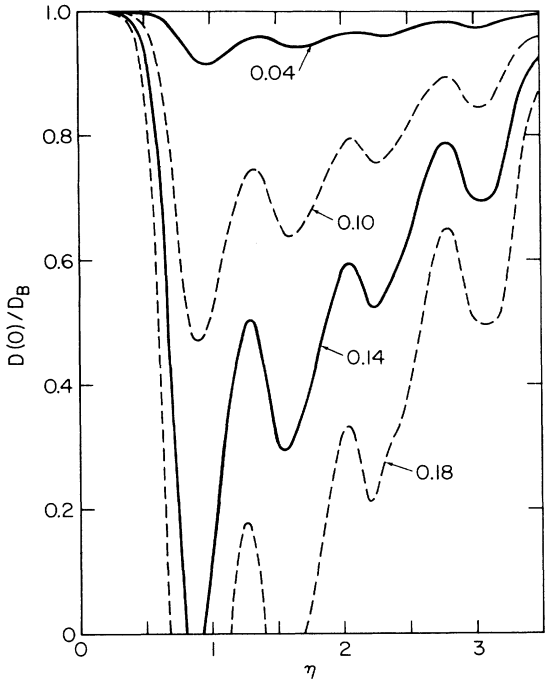

FIG. 6. Diffusion coefficient $D(0)\equiv D(\eta,\omega\to 0)$, scaled by $D_B(\eta)$ for the same case as in Fig. 5. The numbers next to the curves are the corresponding volume fractions n^*.

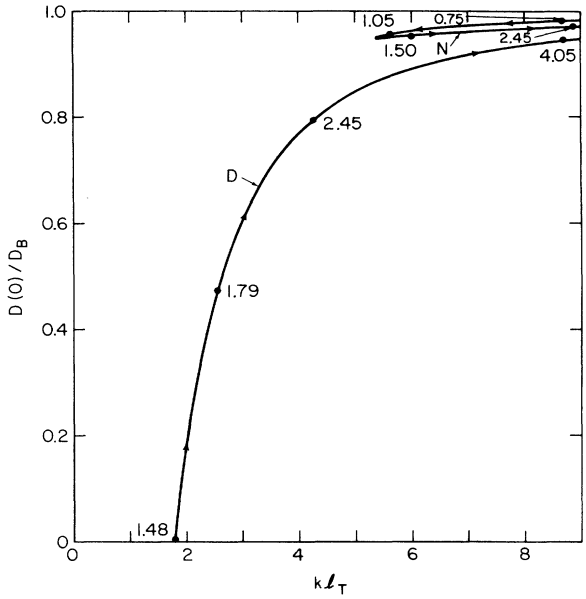

FIG. 7. Evolution of the diffusion coefficient as a function of the Ioffe-Regel product $kl_T=El_T/\bar{c}$ for the Neumann (N) and Dirichlet (D) problems. The density is $n^*=0.155$ and the cutoff is given by $r=2\pi$. The arrows denote the direction of growing η. Some values of η have been specified next to the curves.

Since $\xi(\eta)$ is determined by a superposition of rational combinations of Bessel functions, a series expansion around the mobility edges is possible—in principle—and leads to $\xi\sim|\eta-\eta^{**}|^{-1}$, if we approach the mobility edge η^{**} keeping n^* fixed. This behavior agrees with that obtained in Refs. 1, 2, and 9; a numerical evaluation shows that it can be observed over a reasonably large (typically $\Delta\eta\lesssim 0.01$) neighborhood of η^{**}. The diffusion coefficient also vanishes with an exponent of unity: $D(0)\sim|\eta-\eta^{**}|$. From Eqs. (3.7) and (3.8) we find that the same exponents occur if we approach the mobility edge "vertically" (i.e., varying n^* while keeping η fixed): $D(0)\sim|n^*-n^{**}|$ and $\xi\sim|n^*-n^{**}|^{-1}$.

The Ioffe-Regel criterion, $kl_T=El_T/\bar{c}\approx 1$, can be used as a rough measure of the onset of localization.[27] We can have a more detailed look at this onset if we plot the diffusion coefficient as a function of kl_T. We do this using η as a parameter and observing the evolution of the curve representing $D(0)/D_B$ as η is increased. We show the results for the Dirichlet and Neumann cases in Fig. 7. In the Dirichlet problem there is one mobility edge above which the diffusion coefficient increases monotonically, in agreement with our previous discussions. In the Neumann case, the $D(0)/D_B$ ratio is always close to unity, an indication of the relative weakness of the coherent processes. The multivaluedness of $D(0)$ is typical of the situations when these processes are strongest in an intermediate frequency range.

More interesting is Fig. 8, where we have plotted the results for compressible scatterers; for a full comprehension of this figure, one should look at it in conjunction with Fig. 3 where the horizontal line at $n^*=0.155$ indicates the evolution of η that causes the trajectory in Fig. 8. First, we note that presence of four mobility edges, located at values of kl_T somewhat higher than the Ioffe-Regel estimate. These edges are depicted by the large dots in Fig. 3. The loops in the branch corresponding to

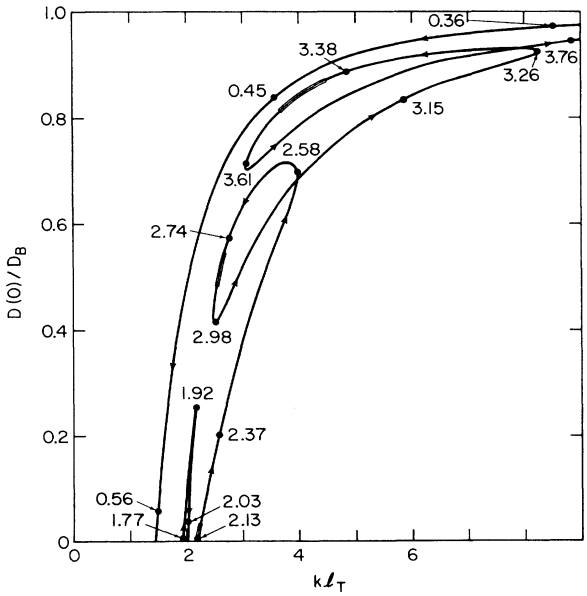

FIG. 8. Evolution of the diffusion coefficient as a function of the Ioffe-Regel product $kl_T=El_T/\bar{c}$ for the case ($\Delta=1$, $M=1.9$). We have chosen $n^*=0.155$ and $r=2\pi$. The arrows denote the direction of growth of the parameter η. Some values of η have been specified next to the curve. The meaning of the three-line segments is discussed in the text.

$\eta > 2.13$ are related to variations in the vertical distance from the $n^* = 0.155$ line to the phase boundary. The segments composed of three thin lines describe regions where the trajectory comes back approximately on itself and then proceeds along its original direction of evolution. For example, the first "triple" region, located in the neighborhood of the fourth mobility edge, is due to the "kink" in the phase boundary at $\eta = 2.25$. We have depicted only the portion of the curve that corresponds to $\eta < 3.77$. Although for higher values of η the trajectory reenters the region $kl_T < 7$, we have chosen not to present the portion of the curve corresponding to $\eta > 3.77$ in order not to obscure the figure.

IV. LOCALIZATION IN $d = 2$

The diffusion coefficient $D(E,\omega \to 0)$ is always zero in two dimensions, and all states are localized. However, it is possible that the localization occurs only on a very large spatial scale; if this scale is bigger than the size of the system or the inelastic attenuation length, the localization effects will not be very relevant. The single-scatterer resonances lead to a considerable shortening of the localization length and suggest the frequency ranges where localization will be strongest.

The formulas we need are again easily obtained from those in I and Ref. 3. Let us first remind the reader of some definitions used in I:

$$\Delta_l(\eta_s) = M\Delta J_l'(\eta_s)[J_l(\eta_s)]^{-1} ,$$
$$\beta_l = J_l'(\eta) - \Delta_l(\eta_s) J_l(\eta) , \tag{4.1}$$

and

$$g_l = Y_l'(\eta) - \Delta_l(\eta_s) Y_l(\eta) .$$

Here J_l and Y_l are cylindrical Bessel functions and the primes denote derivatives with respect to the argument. The formulas for the Neumann case are obtained by writing $\beta_l = J_l'$ and $g_l = Y_l'$; those for the Dirichlet case by letting $\beta_l = J_l$ and $g_l = Y_l$.

The total cross section for an isolated scatterer is

$$S(\eta) = \frac{4a}{\eta} \sum_{l=0}^{\infty} (2-\delta_{l,0}) \frac{\beta_l^2}{\beta_l^2 + g_l^2}$$
$$\equiv \frac{4a}{\eta} T_1(\eta) . \tag{4.2}$$

This function is plotted in Fig. 9 for several types of scatterers. As in the three-dimensional case, an increase in the index of refraction M leads to a richer structure of peaks and valleys. Localization will be favored by the peaks, mostly by those of relatively low frequencies. The large value of S at low frequencies for the Dirichlet problem also generates strong localization in that range. The case $(\Delta = 0.5, M = \sqrt{2})$, corresponding to $\kappa_s = \kappa$ and $\rho_s = 2\rho$ presents a broad maximum at $\eta \cong 4.5$. In spite of the large size of the cross section in that region, there will be no observable localization. For these short wavelengths the excitation propagates from scatterer to scatterer; the strong interactions with the individual scatterers will simply lead to the "normal" diffusion, described by D_B, over scales larger than l_T. The renormalized speed of sound is given by

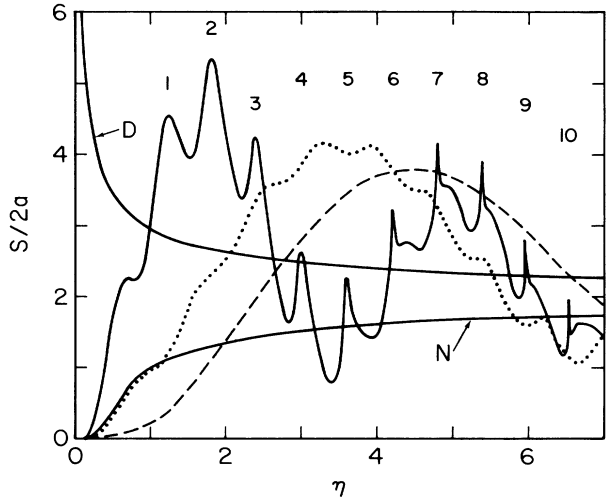

FIG. 9. Total scattering cross section for a disk of radius a as a function of $\eta = Ea/c$. The curves labeled D and N represent the results for Dirichlet and Neumann boundary conditions, respectively. The dotted curves corresponds to $(\Delta = 1, M = 1.5)$ and the dashed curve to $(\Delta = 0.5, M = \sqrt{2})$. The solid curve with the peaks corresponds to $(\Delta = 1, M = 2)$ and the numbers above the peaks give the value of l for the partial wave that resonates. The origin of the small maximum labeled m is discussed in I.

$$\frac{1}{\tilde{c}^2} = \frac{1}{c^2}\left[1 + \frac{4n^*}{\pi\eta^2} \sum_{l=0}^{\infty} \frac{(2-\delta_{l,0})\beta_l g_l}{\beta_l^2 + g_l^2}\right] , \tag{4.3}$$

and the equation for the Boltzmann diffusion coefficient is

$$D_B(\eta) = \frac{\pi a c \eta}{8n^*}\left[\sum_{l=0}^{\infty} \frac{(2-\delta_{l,0})\beta_l^2}{\beta_l^2 + g_l^2} - \frac{2\beta_l\beta_{l+1}(\beta_l\beta_{l+1} + g_l g_{l+1})}{(\beta_l^2 + g_l^2)(\beta_{l+1}^2 + g_{l+1}^2)}\right]^{-1}$$
$$\equiv \frac{\pi a c \eta}{8n^* T_2(\eta)} . \tag{4.4}$$

These functions have been plotted and described in detail in I. As it is the case for the localized states in $d = 3$, the localization length can be obtained from $D(\eta, \omega \to 0)$ using

$$D(\eta, \omega \to 0) = -i\omega\xi^2(\eta) + O(\omega^2) . \tag{4.5}$$

The explicit form for $\xi(\eta)$ is

$$\xi(\eta) = \frac{\pi a \tilde{\eta}}{8rn^* T_2(\tilde{\eta})}\left[\exp\left[\frac{\pi^2\tilde{\eta}^2}{4n^* T_1(\tilde{\eta})}\right] - 1\right]^{1/2} . \tag{4.6}$$

Although the right-hand side is evaluated using $\tilde{\eta} = Ea/\tilde{c}$, in the graphs we will plot ξ as a function of

the source frequency η.

The factor preceding the square root in Eq. (4.6) is l_T/r. This direct proportionality between the localization length and the transport mean free path is a consequence of our choice for the cutoff. Had l_{sc} been chosen instead of l_T, as in Ref. 31, or the PA made as in Ref. 2, the only resulting modification would be the replacement of l_T by l_{sc} in the prefactor in Eq. (4.6). We also see that r appears only as a multiplicative factor. Therefore, the choice of cutoff is less important than in $d=3$.

On the other hand, the appearance of n^* in the exponent generates enormous changes in ξ when the density is modified. This can be seen from Fig. 10, where we have plotted the localization length for the case ($\Delta=1$, $M=2$) (i.e., $\rho_s=\rho$, $\kappa_s=4\kappa$) and several values of n^*. All the curves are seen to have the same general shape, which is determined by single-scattering processes. The minima (maxima) in Fig. 10 are obviously related to the maxima (minima) in Fig. 9. The small distortions, which grow with n^*, are due to the renormalization of the speed of sound.

In Fig. 11 we have plotted the highly structured localization length for very compressible scatterers ($\rho_s=\rho$, $\kappa_s=9\kappa$). Although ξ is always finite, it can change by several orders of magnitude over very narrow frequency intervals. The extremely small ($\xi \lesssim a$) values of the localization length obtained for $\eta<1$ are unphysical, as discussed in Sec. III.

In Fig. 12 we have plotted the localization length for the Dirichlet problem, which shows the expected behav-

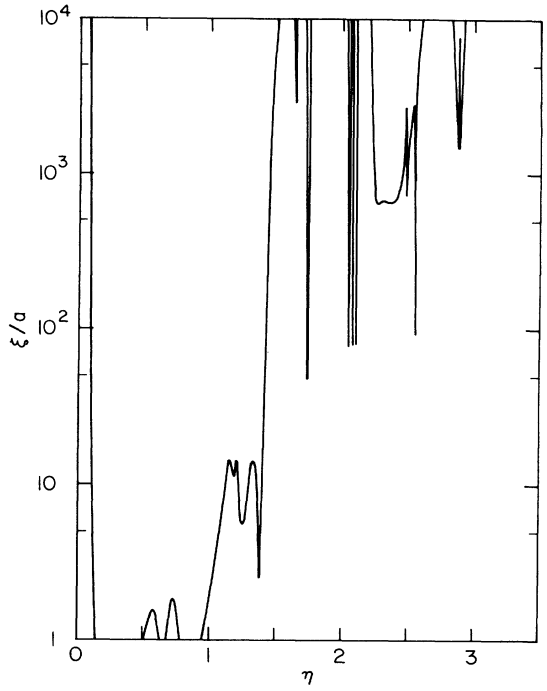

FIG. 11. Localization length for ($\Delta=1$, $M=3$) scatterers. We have chosen $r=2\pi$ and $n^*=0.2$. Features having a width $\Delta\eta<10^{-3}$ have not been indicated.

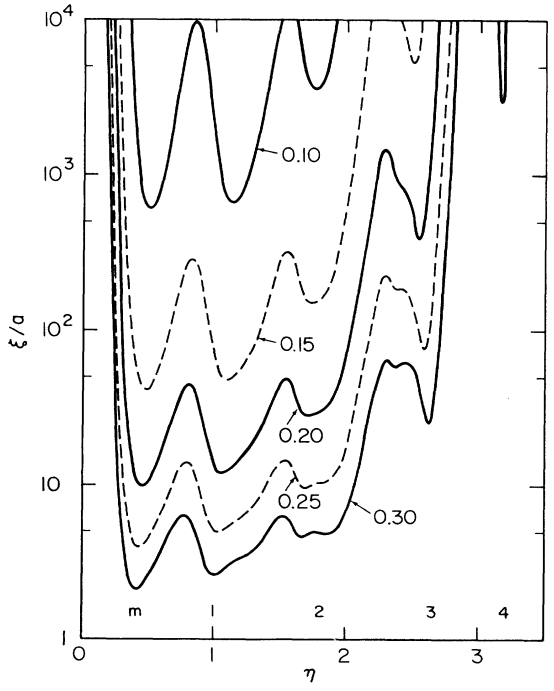

FIG. 10. Localization length for ($\Delta=1$, $M=2$) scatterers. The numbers next to the curves are the corresponding volume fractions n^*. The numbers below indicate which of the resonances in Fig. 9 generates the corresponding minima. We have chosen $r=2\pi$.

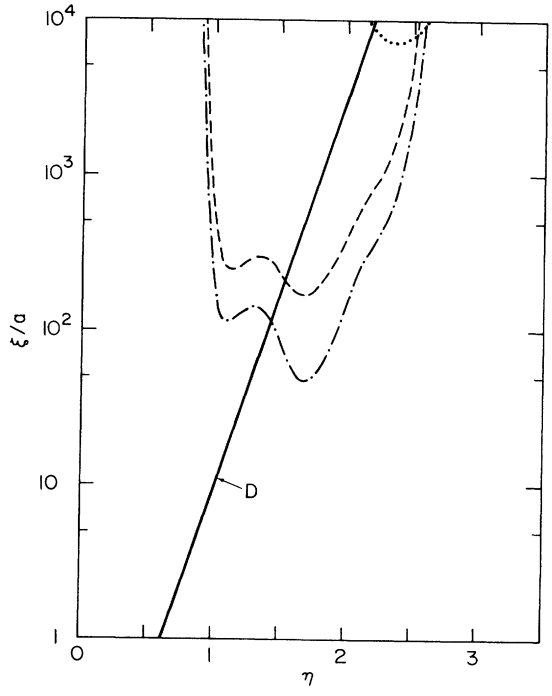

FIG. 12. Localization length for D and permeable scatterers. The dotted line corresponds to ($\Delta=1$, $M=1.5$), the dashed line to ($\Delta=0.25$, $M=2$), and the dotted-dashed line to ($\Delta=0.25$, $M=2$) in the PA approximation. We have taken $n^*=0.2$ and $r=2\pi$.

ior. The localization length for the ($\Delta=1, M=1.5$) case turns out to be very long, showing that even a large maximum in the total cross section (cf. Fig. 9) is not conducive to observable localization effects if it occurs at relatively high frequencies. Similarly, the curve for the ($\Delta=0.5$, $M=\sqrt{2}$) (i.e., $\rho_s=2\rho$) problem does not appear in the graph. If we choose very dense ($\rho_s=4\rho$) scatterers, then the maximum in S is shifted to lower frequencies and we get smaller values for the localization length. For the sake of comparison we have also plotted the results obtained using the PA. As in the $d=3$ problem, the PA overestimates the localization effects but generates the appropriate structure of maxima and minima. The value of ξ for N scatterers is too long to appear in the graph. This case was already analyzed in Ref. 2.

V. DISCUSSION

In this paper we have obtained explicit results for the localization properties of acoustical excitations in media containing random distributions of spherical ($d=3$) or disklike ($d=2$) inclusions. We have considered the cases of hard scatterers, soft scatterers, and scatterers whose densities or compressibilities differ from those of the background. The structure of the curves giving the phase boundary, the localization length and the diffusion coefficient has been related to the properties of the individual scatterers. Several points deserve further remarks.

(1) Undoubtedly, the most interesting case is that of highly compressible scatterers, for which the total cross section for the individual particles presents a rich structure due to partial-wave resonances. These resonances have well-defined effects on the localization properties. To observe these effects, it is necessary for all scatterers to be identical, or nearly so, in composition, shape, and size. Variations in scatterer radius generate a rescaling of the dimensionless frequency η and consequently the position of the peaks in $S(\eta)$ changes from scatterer to scatterer. As the distribution $P(a)$ of the radii is widened, the structure of $n^{**}(\eta)$ and $\xi(\eta)$ becomes more and more smeared out and localization due to resonant scattering weakens.

Fluctuations in scatterer shape also lead to a smearing out of localization effects; in this case, the scattering cross sections for different scatterers cannot be obtained from each other by means of a simple frequency rescaling. Although a similar prediction can be made if one has a distribution of values of κ_s, the results shown in Fig. 3 indicate that some structure will remain, even for a relatively wide distribution.

(2) Let us consider a composite material where the value of n^* for the minority component is near or beyond the percolation threshold, and there is a strong admixture of two waves, each propagating mainly in one of the components. In this case, the structure in the functions describing localization will be smoothed out, even if one of the components is present only under the form of identical spherical particles: the wave that propagates mostly in these spherical inclusions will be scattered by the interstices, which do not have spherical shape. Therefore, the best conditions for the observation of the structures would occur when the scatterers are identical and n^* is reasonably high, but not so much that the wave characteristic of the minority component makes a significant contribution. In this case, we believe our approach gives an essentially correct description, although same smoothing out of sharp features should be expected in view of the occurrence of many scattering events in the near zone of preceding scatterers. If the volume fraction is higher and there is an appreciable amount of admixture, the effective medium approximation used in Ref. 1 is probably better. Under these conditions, however, it appears that the averaging over scatterer shapes would lead to the observation of only two mobility edges.

It should also be mentioned that it may be possible to have substantial admixture even below the percolation threshold. This would be the case, for example, if the minority component is created by a process of aggregation that leads to the formation of long chains or sizable clusters.

(3) Our ignorance of the exact value of the cutoff in the SCT makes our results somewhat imprecise, especially in three dimensions. For this reason, we have made evaluations for several values of the parameter r. We conclude that the frequencies at which the main features in the phase boundary appear depend only weakly on r, although a reduction in r implies that higher values of the scatterer density are needed to obtain similar results. The formulas obtained using an alternative, density-independent cutoff are given in the Appendix.

(4) While in Ref. 31 the cutoff was defined in terms of l_{sc} instead of l_T, in Ref. 2 the cutoff was defined in terms of l_T but then the PA was made. The PA simplifies the calculation because it avoids the computation of D_B and effectively approximates l_T by l_{sc}. We have analyzed how the choices made in Refs. 2 and 31 would modify our predictions. According to the results shown in Figs. 3, 4, and 12, and to the study of the mean free paths made in I, we conclude that, although the magnitude of the localization effects is probably overestimated, the structure generated by the PA is essentially the same as that obtained from the calculation presented here. This confirms the usefulness of the PA. As explained in Ref. 2, it allows a reasonable estimate for problems involving finite-size scattering centers while taking advantage of the simplicity afforded by a Gaussian noise model of the inhomogeneities. The PA can also be applied[42] to the evaluation of the intensity-intensity correlation function.[14]

(5) Flesia *et al.*[15] studied numerically the propagation of classical waves through a network of waveguides with a randomly varying dielectric constant ϵ. They considered (I) a uniform probability distribution of ϵ in the wide interval $[1,1+w]$ and (II) uniform distributions in narrow bands next to 1 and $1+w$ (with probability zero outside of the bands). They conclude that localization effects will be strongest in case (II), which is in agreement with our discussion above. The numerical values for the localization length are very sensitive to the chosen geometry. Consequently, it is not surprising that they predict values of ξ significantly larger than ours.

For $d=2$ they find that localization effects are optimized by selecting the frequency $E\delta/c=1.5$ (δ is the bond length, roughly equivalent to twice our scatterer radius). This is also consistent with our results.

(6) A porous medium is a different kind of disordered system, which may also be appropriate for acoustic localization studies. By the use of a coarse-grained description, Guyer finds that for frequencies above certain mobility edge the excitations must be localized.[43] If there is a minimum scale a' for the pore structure (i.e., if the material is not a true fractal), our discussion indicates that a second mobility edge should appear at a frequency $E'\sim c/a'$. Below this edge the sound waves would start diffusing again.

(7) Let us finally point out that the problem treated in Ref. 4 is the one-dimensional counterpart of the problem discussed in this paper. The main difference is that in one dimension there are special frequencies at which these scatterers become perfectly transparent and thus extended states are possible. Those transmission resonances cannot occur in higher-dimensionality systems because the total cross section never vanishes at a nonzero frequency.

ACKNOWLEDGMENTS

This research was supported in part by the National Science Foundation through Grants Nos. PHY 83-51473 and DMR 86-07605.

APPENDIX: AN ALTERNATIVE CUTOFF

As stated at the end of Sec. II, another possible choice for the momentum cutoff is $Q=r/a$. It is easy to write the formulas that are generated by this option. A general observation is that, since D_B enters the equations in the main body of the paper through the cutoff, it will not appear here (except as the obvious prefactor in the diffusion coefficient).

In two dimensions, the equation for the localization length is

$$\xi(\eta)=\frac{a}{r}\left[\exp\left[\frac{\pi^2\tilde{\eta}^2}{4n^*T_1(\tilde{\eta})}\right]-1\right]^{1/2}. \tag{A1}$$

The quantitative differences with Eq. (4.6) may be noticeable, mostly at small values of n^*.

The three-dimensional case is more interesting. The phase boundary is given by

$$n^{**}=\pi\tilde{\eta}^4/9rS_1 . \tag{A2}$$

Choosing $Q\sim l_T^{-1}$ yielded [see Eq. (3.5)] $n^{**}\sim\tilde{\eta}^3(rS_1S_2)^{-1/2}$. Consequently, the choice of r is more critical here. The localization length solves the transcendental equation

$$\left[1-\frac{\pi\eta^4}{9n^*rS_1}\right]\frac{r\xi}{a}=\arctan\left[\frac{r\xi}{a}\right]. \tag{A3}$$

Note that if we take $Q\sim l_T^{-1}\sim n^*$ in Eq. (3.7) we obtain an $(n^*)^2$ factor in the denominator of the second term inside the brackets. This different dependence on the volume fraction is even more obvious in the equation for the diffusion coefficient, which reads as

$$D(0)=D_B\left[1-\frac{9rn^*S_1}{\pi\tilde{\eta}^4}\right]. \tag{A4}$$

The linear (in n^*) correction to D_B results whenever the cutoff is chosen to be independent of the scatterer volume fraction. Aside from the modifications just discussed, the qualitative features of the graphs resulting from the choices $Q=r/a$ and $Q=rcD_B^{-1}$ are generally similar.

*Present address: Fakultät für Physik, Universität Konstanz, D-7750 Konstanz 1, West Germany.

[1]P. Sheng and Z. Q. Zhang, Phys. Rev. Lett. **57**, 1879 (1986).
[2]C. A. Condat and T. R. Kirkpatrick, Phys. Rev. Lett. **58**, 226 (1987).
[3]C. A. Condat (unpublished).
[4]C. A. Condat and T. R. Kirkpatrick, Phys. Rev. B **33**, 3102 (1986).
[5]C. Dépollier, J. Kergomard, and F. Laloe, Ann. Phys. (Paris) **11**, 457 (1986).
[6]S. He and J. D. Maynard, Phys. Rev. Lett. **57**, 3171 (1986).
[7]C. A. Condat and T. R. Kirkpatrick, Phys. Rev. B **32**, 495 (1985).
[8]S. John, H. Sompolinsky and M. J. Stephen, Phys. Rev. B **27**, 5592 (1983).
[9]T. R. Kirkpatrick, Phys. Rev. B **31**, 5746 (1985).
[10]D. Vollhardt and P. Wölfle, Phys. Rev. B **22**, 4666 (1980). For an earlier and similar approach, see W. Götze, Solid State Commun. **27**, 1393 (1978).
[11]S. Cohen and J. Machta, Phys. Rev. Lett. **54**, 2242 (1985).
[12]S. Cohen, J. Machta, T. R. Kirkpatrick, and C. A. Condat, Phys. Rev. Lett. **58**, 785 (1987).
[13]C. A. Condat, T. R. Kirkpatrick, and S. Cohen, Phys. Rev. B **35**, 4653 (1987).
[14]B. Shapiro, Phys. Rev. Lett. **57**, 2168 (1986).
[15]C. Flesia, R. Johnston, and H. Kunz, Europhys. Lett. **3**, 497 (1987).
[16]Y. Kuga and A. Ishimaru, J. Opt. Soc. Am. A **1**, 831 (1984).
[17]A. van Albada and A. Lagendijk, Phys. Rev. Lett. **55**, 2692 (1985).
[18]P. E. Wolf and G. Maret, Phys. Rev. Lett. **55**, 2696 (1985).
[19]A. Lagendijk, M. van Albada, and M. B. van der Mark, Physica **140A**, 183 (1986).
[20]S. Etemad, R. Thomson, and M. J. Andrejco, Phys. Rev. Lett. **57**, 575 (1986).
[21]M. Kaveh, M. Rosenbluh, I. Edrei, and I. Freund, Phys. Rev. Lett. **57**, 2048 (1986).
[22]M. van Albada, M. B. van der Mark, and A. Lagendijk, Phys. Rev. Lett. **58**, 361 (1987).
[23]A. Z. Genack, Phys. Rev. Lett. **58**, 2043 (1987).

[24]Yu. A. Kravtsov and A. I. Saichev, Usp. Fiz. Nauk. **137**, 501 (1982) [Sov. Phys.—Usp. **25**, 494 (1982)]. This is an excellent review of the theoretical and experimental status of the subject of enhanced backscattering by 1982.

[25]A. A. Golubentsev, Zh. Eksp. Teor. Fiz. **86**, 47 (1984) [Sov. Phys.—JETP **69**, 26 (1984)].

[26]S. John, Phys. Rev. Lett. **53**, 2169 (1984).

[27]P. W. Anderson, Philos. Mag. B **52**, 505 (1985).

[28]L. Tsang and A. Ishimaru, J. Opt. Soc. Am. A **2**, 2187 (1985).

[29]E. Akkermans, P. E. Wolf, and R. Maynard, Phys. Rev. Lett. **56**, 1471 (1986).

[30]M. J. Stephen and G. Cwilich, Phys. Rev. B **34**, 7564 (1986).

[31]K. Arya, Z. B. Su, and J. L. Birman, Phys. Rev. Lett. **57**, 2725 (1986).

[32]The effect of dissipation in the case of electromagnetic excitations in a medium containing conducting spheres was underestimated in Ref. 2. To make a meaningful comparison with the localization length, the absorption length l_i should be measured radially and not along the actual path of the excitation. Therefore, if $\pi a^2 Q_{ab}$ is the absorption cross section, $l_i \sim a(n^* Q_{ab})^{-1/2}$. The numerical estimates should there be changed to $l_i \sim 20a$ and $l_i \sim 3a$ for the ir and uv ranges, respectively. Dissipation will probably make localization by conducting spheres all but unobservable in the uv range.

[33]C. M. Davis, L. R. Dragonette, and L. Flax, J. Acoust. Soc. Am. **63**, 1694 (1978).

[34]U. Frisch, in *Probabilistic Methods in Applied Mathematics,* edited by A. T. Bharucha-Reid (Academic, New York, 1968), Vol. I.

[35]K. M. Watson, J. Math. Phys. **10**, 688 (1969).

[36]D. A. de Wolf, IEEE Trans. Antennas Propag. **AP-19**, 254 (1971).

[37]Y. N. Barabanenkov, Izv. Vyssh. Uchebn. Zaved. Radiofiz. **16**, 88 (1973); Usp. Fiz. Nauk. **117**, 49 (1975) [Sov. Phys.—Usp. **18**, 673 (1976)]. The importance of the MCD's was first pointed out, in a different context, by J. S. Langer and T. Neal, Phys. Rev. Lett. **16**, 984 (1966).

[38]See, for example, B. L. Altshuler, A. G. Aronov, D. E. Khmelnitskii, and A. J. Larkin, in *Quantum Theory of Solids,* edited by I. M. Lifshitz (Mir, Moscow, 1982); G. Bergmann, Physica **126B**, 229 (1984); D. E. Khmelnitskii, *ibid.* **126B**, 235 (1984).

[39]V. L. Berezinskii, Zh. Eksp. Teor. Fiz. **65**, 1251 (1973) [Sov. Phys.—JETP **38**, 620 (1974)].

[40]A. D. Zdetsis, C. M. Soukoulis, E. N. Economou, and G. S. Grest, Phys. Rev. B **32**, 7811 (1985).

[41]T. R. Kirkpatrick and D. Belitz, Phys. Rev. B **34**, 2168 (1986).

[42]C. A. Condat, Phys. Rev. Lett. **59**, 606 (1987).

[43]R. A. Guyer (unpublished).